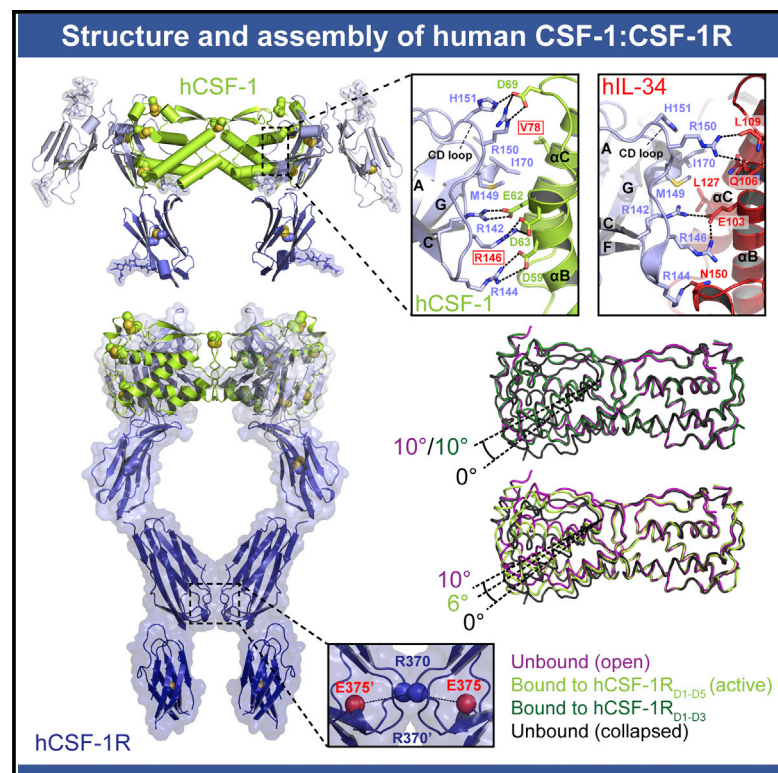# Structure and Assembly Mechanism of the Signaling Complex Mediated by Human CSF-1

Graphical Abstract

Authors

Jan Felix, Steven De Munck, Kenneth Verstraete, ..., Nico Callewaert, Jonathan Elegheert, Savvas N. Savvides

Correspondence

savvas.savvides@ugent.be

In Brief

Signaling pathways initiated by colony-stimulating factor 1 receptor (CSF-1R) play pivotal roles in immunity, inflammation, and cancer. Felix et al. reconstruct the stepwise assembly mechanism of the protein complex underlying the activation of human CSF-1R using crystal structures of the receptor in complex with its activating cytokine, CSF-1.

Highlights

- Structures of human CSF-1 in complex with CSF-1R

- Plasticity of dimeric hCSF-1 enables an active cytokine state

- Cytokine-binding duality of human CSF-1R exposed

- Detailed mechanistic proposal for the activation of human CSF-1R

Accession Numbers

4WRL
4WRM

CrossMark

CellPress

Article

Structure and Assembly Mechanism of the Signaling Complex Mediated by Human CSF-1

Jan Felix,[1,2,4] Steven De Munck,[1,2,4] Kenneth Verstraete,[1,2] Leander Meuris,[1,3] Nico Callewaert,[1,3] Jonathan Elegheert,[1,5] and Savvas N. Savvides[1,2,*]

[1]Laboratory for Protein Biochemistry and Biomolecular Engineering (L-ProBE), Department of Biochemistry and Microbiology, Ghent University, 9000 Ghent, Belgium
[2]Unit for Structural Biology, VIB Inflammation Research Center, 9052 Ghent, Belgium
[3]VIB Medical Biotechnology Center, 9052 Ghent, Belgium
[4]Co-first author
[5]Present address: Division of Structural Biology, Wellcome Trust Center for Human Genetics, University of Oxford, UK
*Correspondence: savvas.savvides@ugent.be
http://dx.doi.org/10.1016/j.str.2015.06.019

SUMMARY

Human colony-stimulating factor 1 receptor (hCSF-1R) is unique among the hematopoietic receptors because it is activated by two distinct cytokines, CSF-1 and interleukin-34 (IL-34). Despite ever-growing insights into the central role of hCSF-1R signaling in innate and adaptive immunity, inflammatory diseases, and cancer, the structural basis of the functional dichotomy of hCSF-1R has remained elusive. Here, we report crystal structures of ternary complexes between hCSF-1 and hCSF-1R, including their complete extracellular assembly, and propose a mechanism for the cooperative human CSF-1:CSF-1R complex that relies on the adoption by dimeric hCSF-1 of an active conformational state and homotypic receptor interactions. Furthermore, we trace the cytokine-binding duality of hCSF-1R to a limited set of conserved interactions mediated by functionally equivalent residues on CSF-1 and IL-34 that play into the geometric requirements of hCSF-1R activation, and map the possible mechanistic consequences of somatic mutations in hCSF-1R associated with cancer.

INTRODUCTION

The hematopoietic colony-stimulating factor 1 receptor (CSF-1R) Sherr et al. (1985), a class III receptor tyrosine kinase (RTKIII) (Lemmon and Schlessinger, 2010), is pivotal to the survival, proliferation, and differentiation of mononuclear phagocytic cells such as monocytes, tissue macrophages, muscularis macrophages, microglia, osteoclasts, Paneth cells, and myeloid dendritic cells (Muller et al., 2014; Stanley and Chitu, 2014; Verstraete and Savvides, 2012). CSF-1R is activated by two distinct cytokines, colony-stimulating factor 1 (CSF-1) and inter-eukin-34 (IL-34) (Lin et al., 2008) which, despite their disparate sequences, adopt similar four-helix bundle folds (Ma et al., 2012; Pandit et al., 1992). While CSF-1 and IL-34 share similar

biological activities (Wei et al., 2010), they differ in their signaling patterns through CSF-1R (Chihara et al., 2010) and in terms of spatiotemporal expression levels (Nandi et al., 2012; Wei et al., 2010).

Binding of CSF-1 or IL-34 to the extracellular segment of CSF-1R elicits dimerization and intracellular autophosphorylation of CSF-1R to initiate intracellular signaling. Such an activation theme is common among all other RTKIII family members, including KIT, Fms-like tyrosine kinase 3 receptor (Flt3) and platelet-derived growth factor receptor α/β (PDGFR α/β) (Verstraete and Savvides, 2012). RTKIIIs share a common architecture consisting of five extracellular immunoglobulin-like domains, a transmembrane helix, and an intracellular autoinhibitory juxtamembrane domain linked to split tyrosine kinase domains. The involvement of RTKIIIs in a plethora of cellular processes central to innate and adaptive immunity has inevitably linked aberrant RTKIII signaling to numerous inflammatory diseases and cancer. For instance, altered CSF-1R signaling is implicated in widespread human pathologies such as rheumatoid arthritis, atherosclerosis, tumor growth, and metastasis (Chitu and Stanley, 2006; Masteller and Wong, 2014; Pollard, 2009; Stanley and Chitu, 2014; Verstraete and Savvides, 2012).

Due to the emerging dichotomy of CSF-1R signaling via two distinct cytokines with restrictive species cross-reactivity and the rising therapeutic importance of CSF-1R signaling (Hume and MacDonald, 2012; Ries et al., 2014; Stanley and Chitu, 2014), the need to dissect the structural and mechanistic principles underlying cytokine-CSF-1R assemblies has been more acute than ever. Recent structural undertakings focusing on crystallographic structures of partial CSF-1R complexes (Chen et al., 2008; Liu et al., 2012; Ma et al., 2012) have provided significant momentum in this direction and have fueled the modeling of complete extracellular assemblies mediated by human IL-34 (hIL-34) and CSF-1 (hCSF-1) via electron microscopy (EM) and small-angle X-ray scattering (SAXS) (Elegheert et al., 2011; Felix et al., 2013). In addition, structural insights into the allosteric inactivation of hCSF-1 by the viral decoy receptor BARF1 (Elegheert et al., 2012) highlighted the possible relevance of inter-subunit plasticity of CSF-1 in CSF-1R activation. However, structures of hCSF-1 in complex with hCSF-1R at high resolution had remained as the missing link to a robust mechanistic proposal for hCSF-1 driven activation of human CSF-1R.

In this study, we present a series of structural insights derived from crystal structures of ternary complexes of hCSF-1 with its cognate receptor that, together with a plethora of available structure-function studies, lead to a stepwise delineation of the mechanistic principles underlying the assembly of the extracellular hCSF-1:CSF-1R complex. In particular, we show that the inherent structural plasticity of dimeric hCSF-1 is critical for the assembly of the cooperative hCSF-1:CSF-1R signaling complex, offering new insight into the role of cytokine-mediated activation of hematopoietic receptors. In addition, our work provides a structural platform to rationalize the possible impact of somatic mutations in the ectodomain of hCSF-1R and sets the stage for further mechanistic and therapeutic interrogation of hCSF-1R and hCSF-1.

RESULTS

Structure of the Ternary Encounter Complex Mediated by hCSF-1

Structural characterization of complexes between hematopoietic cytokines and truncated constructs of the extracellular segments of their cognate RTKIII have served as key puzzle pieces to dissect the structural and mechanistic principles underlying the assembly of their signaling complexes (Verstraete and Savvides, 2012). However, in the case of CSF-1R, crystal structures of mouse CSF-1R$_{D1-D3}$ in complex with mouse CSF-1 (Chen et al., 2008) and hIL-34 in complex with hCSF-1R$_{D1-D3}$ (Ma et al., 2012) revealed binary (1:1) cytokine-receptor complexes wherein the dimeric cytokine was bound by a single receptor molecule. Such a stoichiometry was inconsistent with ternary assemblies, in which the dimeric cytokine is bound by two molecules of the receptor, as revealed by orthogonal structural studies (Elegheert et al., 2011; Felix et al., 2013) and biochemical and biophysical methods (Elegheert et al., 2011; Felix et al., 2013; Ma et al., 2012). As was elegantly shown for the hIL-34:CSF-1R$_{D1-D3}$ complex, this discrepancy could be traced to the crystallization process whereby one molecule of hCSF-1R$_{D1-D3}$ disengages from the ternary complex, leading to a binary complex in the ensuing crystal form (Ma et al., 2012).

To obtain diffraction-quality crystals that would enable elucidation of the hitherto elusive ternary complex of hCSF-1 with hCSF-1R$_{D1-D3}$ and the cytokine-receptor interfaces at high resolution, we engineered point mutations at each of the four known N-linked glycosylation sites in hCSF-1R$_{D1-D3}$ (Ma et al., 2012) (N73, N153, N240, N275) and initially expressed the four hCSF-1R$_{D1-D3}$ variants in HEK293T and HEK293S GnTI$^{-/-}$ cells (Reeves et al., 2002). In addition, we employed the recently developed HEK293S-GlycoDelete cell line, which produces proteins with homogeneous N-linked glycans of the form GlcNAc-Gal-Sia (Meuris et al., 2014). Ternary hCSF1:CSF-1R$_{D1-D3}$ complexes were reconstituted and purified after mixing a molar excess of recombinant hCSF-1 (Elegheert et al., 2011; Verstraete et al., 2009) with hCSF-1R$_{D1-D3}$ glycosylation variants and were further confirmed in terms of stoichiometry by size-exclusion chromatography (SEC) combined with multi-angle light-scattering measurements (Elegheert et al., 2011; Felix et al., 2013).

The crystal structure of the hCSF-1:CSF1R$_{D1-D3}$ ternary complex was determined to 2.8 Å resolution from crystals grown using hCSF-1R$_{D1-D3}$ carrying the N240Q point mutation pro-

duced in HEK293S-GlycoDelete cells (Table 1; Experimental Procedures). The best diffracting crystals were obtained from hCSF-1R$_{D1-D3}$ expressed in the GlycoDelete cell line (Meuris et al., 2014), highlighting the possible advantages of short and homogeneous N-linked glycans for lattice formation and crystal growth. Indeed, the crystal asymmetric unit contains a ternary complex with one hCSF-1 dimer bound by two hCSF-1R$_{D1-D3}$ molecules 65 Å apart at the two ends of the hCSF-1 dimer (Figure 1A). Human CSF-1R$_{D1-D3}$ employs a nearly linear arrangement of D2 and D3 to form the binding site for hCSF-1, while D1 adopts a collapsed conformation about the D1-D2 linker region to interact with D2, in contrast to the extended conformation observed in solution via SAXS and EM (Elegheert et al., 2011; Felix et al., 2013). Generating a ternary complex for human IL-34:CSF-1R$_{D1-D3}$ based on the crystal structure of the binary complex (Ma et al., 2012) reveals that the two complexes are macroscopically indistinguishable (Figure 1B), consistent with recent comparative studies of the two complexes at low resolution (Felix et al., 2013) and the structure of mouse IL-34 in complex with CSF-1R$_{D1-D3}$ (Liu et al., 2012). Each hCSF-1R$_{D1-D3}$ molecule in the hCSF-1:CSF1R$_{D1-D3}$ complex is decorated by four N-linked GlcNAc-Gal-Sia glycans, three at the expected sites (N53, N153 and N275) and one at a newly identified site (N45) (Figure 1A). We note that the absence of N-linked glycosylation at position 240 due to the N240Q mutation enables crystal-packing contacts between symmetry-related D3 domains, while the glycans at N153 and N275 interact via van der Waals contacts with the corresponding glycan trees in symmetry-related receptor molecules. Moreover, we observed a α1-6 linked fucose on the GlcNAc glycan residue at N73. The presence of core fucosylation had been previously anticipated for proteins produced in the GlycoDelete cell line (Meuris et al., 2014) but had hitherto not been observed experimentally.

Thus, we now provide direct structural evidence at high resolution that hCSF-1 is able to establish a ternary complex with hCSF-1R$_{D1-D3}$, thereby corroborating biophysical (Elegheert et al., 2011; Ma et al., 2012) and structural studies in solution at low resolution (Elegheert et al., 2011; Felix et al., 2013). Importantly, we can now conclude that D4 and D5, the membrane-proximal domains of hCSF-1R, are not a requisite for the formation of a ternary complex with either of its cognate cytokines. This provides insights into a central mechanistic role for an initial ternary encounter complex mediated by hCSF-1 and hIL-34 to nucleate receptor dimerization and a signaling complex.

Structural Basis of the Cytokine-Binding Duality of hCSF-1R

The herein presented structural details of the hCSF-1:CSF-1R binding interface and the previously determined hIL-34:CSF-1R interaction landscape (Ma et al., 2012) allow tracing of the functional dichotomy of hCSF-1R to structural considerations and rationalization of available mutagenesis data.

The hCSF-1:CSF-1R interface buries ~1900 Å^2 of solvent-accessible surface area distributed over two almost equally extensive epitopes on hCSF-1R, termed hereafter as site I and site II (Figure 1C; Table S1). The two interaction epitopes are physically divided by the D2-D3 linker, which does not participate in hCSF-1 binding. Site I is hosted by D2 in hCSF-1R and

Table 1. Crystallographic Data Collection and Refinement Statistics

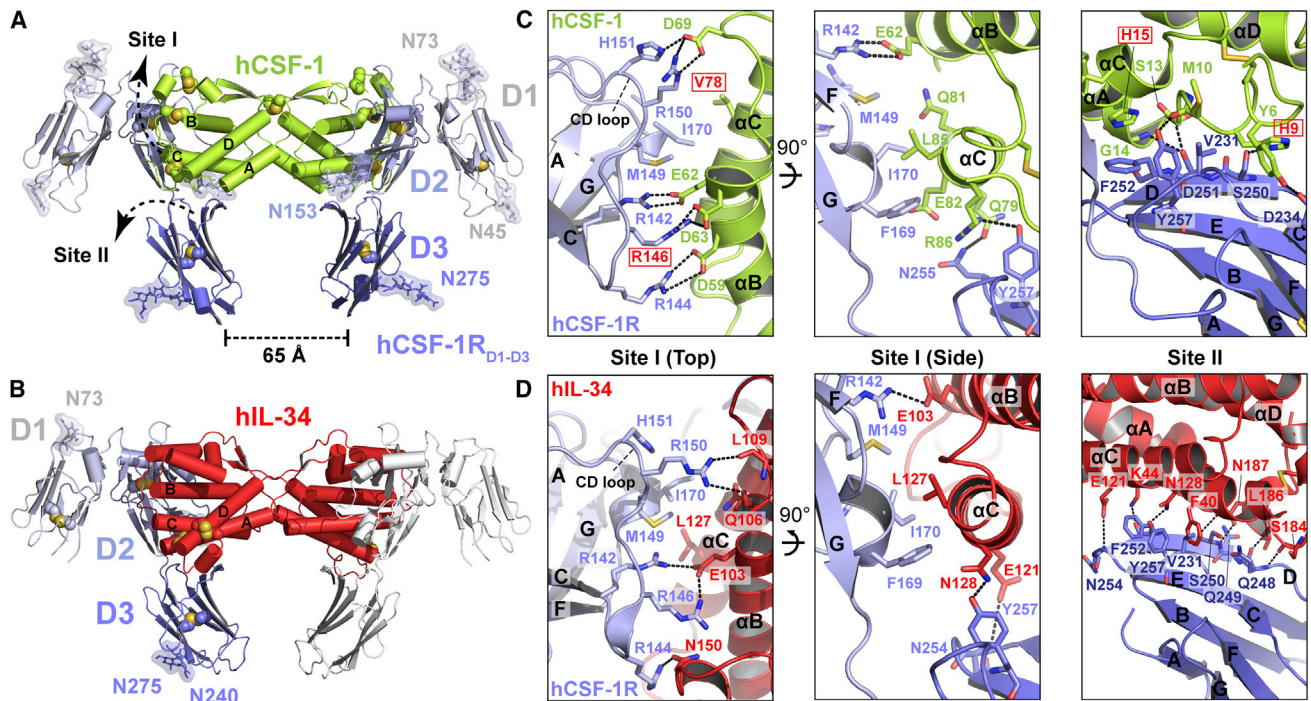|	hCSF-1:CSF-1R$_{D1–D3}$ N240Q	hCSF-1:CSF-1R$_{D1–D5}$	hCSF-1:CSF-1R$_{D1–D5}$ Corrected for Anisotropy[a]
Data Collection			
Beamline	ID23-1 (ESRF, France)	PXI (SLS, Switzerland)	PXI (SLS, Switzerland)
Space group	$I4_1$	$P6_122$	$P6_122$
Cell dimensions			
a, b, c (Å)	143.00, 143.00, 138.323	281.47, 281.47, 91.17	281.47, 281.47, 91.17
α, β, γ (°)	90, 90, 90	90, 90, 120	90, 90, 120
Resolution (Å)	49.71–2.80 (2.97–2.80)	48.75–6.80 (7.21–6.80)	48.75–6.83 (7.01–6.83)
Unique reflections	34,125 (5,448)	3,953 (610)	3,285 (38)
R_{meas} (%)	6.4 (81.5)	7.1 (102.8)	5.9 (30.8)
$<I/\sigma(I)>$	20.73 (2.32)	21.33 (2.89)	25.71 (6.67)
Completeness (%)	99.8 (99.2)	99.5 (100)	83.8 (13.1)
Multiplicity	6.9 (6.8)	10.2 (10.4)	9.9 (7.8)
Wilson B factor (Å^2)	82.3	463.7	238.5
Refinement			
Resolution (Å)	49.71–2.80	48.75–6.80	48.75–6.80
R_{work}/R_{free} (%)	22.31/26.13	34.29/36.19[b]	32.93/35.93
No. of atoms			
Total	6,657	4,524	4,524
Protein	6,370	4,524	4,524
Glycan	287	–	–
Average B factor (Å^2)	100.3	313.7	313.7
Protein B factor (Å^2)	97.4	313.7	313.7
Glycan B factor (Å^2)	164.6	–	–
Root-mean-square deviations			
Bonds (Å)	0.006	0.008	0.008
Angles (°)	1.094	1.200	1.200
Ramachandran favored (%)	95.6	96.1	96.1
Ramachandran outliers (%)	0	0	0
PDB	4WRL	4WRM[b]	4WRM

Values in parentheses correspond to the highest-resolution shell.
[a]Ellipsoidal truncation and anisotropic scaling of the data were performed using the Diffraction Anisotropy Server (Strong et al., 2006).
[b]Structure PDB: 4WRM (refined against anisotropy corrected data) validated against full data range.

comprises the CD and EF loops, which interact with helices B en C on hCSF-1. On the other hand, site II localizes on D3 of hCSF-1R and is defined by the BC loop and β strands D and E, which engage helix A and the N-terminal loop of hCSF-1. Site I is dominated by polar interactions mediated by a basic patch on the BC loop of hCSF-1R$_{D2}$ defined by R142, R144, and R146 forming salt bridge networks with E62, D59, and D63 on helix B of hCSF-1, respectively (Figure 1C, site I; Table S1). On the periphery of the BC loop a second set of basic residues, R150 and H151, interact with D69 on hCSF-1 (Figure 1C, site I; Table S1). Near the bottom of site I adjacent to the D2-D3 hinge region, V78 and L85 on helix C of hCSF-1 interact with I170 and F169 on hCSF-1R, respectively. Fittingly, V78 in hCSF-1 had previously been identified as a functional hotspot (Taylor et al., 1994). The latter is further engaged in a cation-π interaction with R86, which in turn makes a hydrogen bond with the hydroxyl group of Y252 (Figure 1C, side view site I; Table S1). Site II is formed by β strands D and E and the BC loop of hCSF-1R$_{D3}$,

which interact with helix C and the N-terminal part of helix A of hCSF-1 (Figure 1C, site II; Table S1). This site mainly features two hydrogen bond-rich regions separated by V231 on the BC loop of hCSF-1R$_{D3}$. This residue is flanked by Y257 on hCSF-1R$_{D3}$ and Y6 on hCSF-1 and makes van der Waals contacts with M10 on hCSF-1. The first set of hydrogen bonds is formed between the hydroxyl group of Y257 on strand E of hCSF-1R$_{D3}$ and the backbone carbonyl oxygen of M10 on hCSF-1, and between D251 on strand D of hCSF-1R$_{D3}$ and the backbone amide hydrogen atoms of S13 and G14 (Figure 1C, site II; Table S1). The second hydrogen bond network consists of S250 on strand D of hCSF-1R$_{D3}$ making hydrogen bonds with H9 on hCSF-1, and between D234 at the end of the BC loop of hCSF-1R$_{D3}$ and Y6 at the N terminus of hCSF-1. Near the D2-D3 hinge, F252 on hCSF-1R$_{D3}$ marks the boundary of site II by engaging in a π-π stacking interaction with H15 on helix A of hCSF-1 (Figure 1C, site II; Table S1). Indeed, H9 and H15 in hCSF-1 were previously identified as binding and functional hotspots (Taylor et al., 1994).

Figure 1. Crystal Structure of the hCSF-1:CSF-1R$_{D1-D3}$ Ternary Complex

(A) Dimeric hCSF-1 (lemon green) recruits two hCSF-1R$_{D1-D3}$ receptor molecules (light to dark blue). Disulfide bridges are shown as spheres, and glycans in hCSF-1R$_{D1-D3}$ are shown as sticks and transparent surfaces.

(B) The hIL-34 dimer (red) binds to only one hCSF-1R$_{D1-D3}$ receptor molecule (light to dark blue) (PDB: 4DKD) (Ma et al., 2012). The second hCSF-1R$_{D1-D3}$ molecule, shown in white, was modeled for comparison purposes.

(C and D) Insets show a detailed view of the hCSF-1:hCSF-1R$_{D1-D3}$ (C) and hIL-34:CSF-1R$_{D1-D3}$ (D) binding epitopes. Functional hotspots in hCSF-1 (H9, H15, and V78) (Taylor et al., 1994), and mouse CSF-1R (R146) (Chen et al., 2008) are labeled in red (C).

See also Figure S1 and Table S1.

Substitution of additional residues beyond this point along helix A (Q17, Q20, and R21) does not affect binding of hCSF-1 (Taylor et al., 1994), which can now be readily explained by the lack of involvement of these residues in the binding interface.

Remarkably, despite the absence of sequence similarity between the two hCSF-1R ligands, the two cytokines target exactly the same residues in site I of the hCSF-1R binding interface, albeit each deploying a different set of interacting residues (Figures 1C and 1D). For instance, R142 and R146 in hCSF-1R$_{D2}$ interact electrostatically with E103 in hIL-34 versus E62 and D63 in hCSF-1 (site I, Figure 1C). Substitution of R146, a conserved residue in CSF-1R$_{D2}$ across species, to alanine in mouse CSF-1R$_{D2}$, abrogates binding to CSF-1 (Chen et al., 2008), supporting a central role for this residue in the cytokine-binding duality of CSF-1R. Furthermore, R144 and R150 in hCSF-1R interact with the main-chain carbonyl oxygen of N150, Q106, and L109 in hIL-34 (site I, Figure 1D), as opposed to engaging in salt bridge networks with D69 and D59 in hCSF-1 (site I, Figure 1C). The level of congruence observed among the respective site I interfaces in hCSF-1 and hIL-34 mediated complexes is only partly copied to site II. This is because the site II interface mediated by hIL-34 is augmented by additional interactions involving N254 and Q249 and displays a far more extensive hydrogen network than the hCSF-1:CSF-1R site II interaction (Figure 1D, site II). That such structural differ-

ence centers localizes on hCSF-1R$_{D3}$ would be consistent with the emerging notion that D3 may be in evolutionary terms the primordial cytokine-binding domain in the RTKIII family of receptors (Verstraete and Savvides, 2012).

hCSF-1R$_{D3}$ Displays Structural Plasticity

Given the convergent evolution of hCSF-1 and hIL-34 to exploit very similar binding principles hosted by their cognate receptor, we wondered whether hCSF-1R$_{D3}$ might contribute to binding specificity in any additional ways. When the two copies of hCSF-1R$_{D1-D3}$ in the ternary hCSF-1:CSF-1R$_{D1-D3}$ complex are superimposed with hCSF-1R$_{D1-D3}$ from the binary hIL-34:CSF-1R$_{D1-D3}$ complex based on an alignment of the D1-D2 module, several surprising features become apparent. Firstly, D3 in one of the two receptor molecules in the hCSF-1:hCSF-1R$_{D1-D3}$ ternary assembly is rotated by ~15° around the D2-D3 hinge, breaking down the apparent 2-fold symmetry of the hCSF-1:CSF-1R$_{D1-D3}$ ternary complex (Figure S1A). While this results in a relatively small positional shift near the D2-D3 hinge region, it is far more pronounced at the extremities of D3. Secondly, despite such a pronounced conformational difference between the two copies of hCSF-1R$_{D1-D3}$, the respective interaction interfaces with hCSF-1 are virtually superimposable (Figure S1B). Lastly, when we incorporate hCSF-1R$_{D1-D3}$ as bound to hIL-34 into our analysis, we observe yet a third distinct conformation
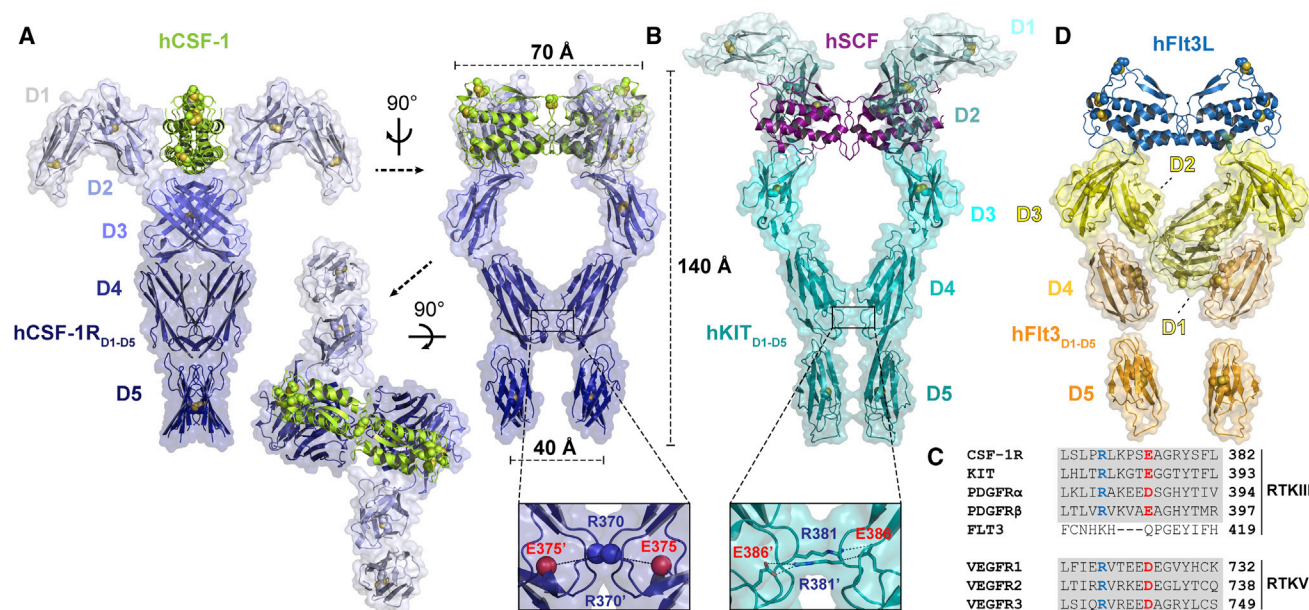
Figure 2. Crystal Structure of the hCSF-1:CSF-1R$_{D1-D5}$ Extracellular Complex

(A) Cartoon representation of the ternary complex between hCSF-1 (lemon green) and the full hCSF-1R ectodomain (light to dark blue). Disulfide bridges in hCSF-1 and hCSF-1R$_{D1-D5}$ are shown as spheres. The inset zooms into the D4-D4′ interface, with Cα atoms of R370 and E375 shown as spheres.

(B) Cartoon representation of the human SCF:KIT complex (PDB: 2E9W) (Yuzawa et al., 2007). The inset zooms into D4-D4′ contacts in KIT.

(C) Alignment of conserved D4 sequences from human CSF-1R, KIT, PDGFR-α, PDGFR-β, and Flt3.

(D) Cartoon representation of the human Flt3L:Flt3 complex (PDB: 3QS9) (Verstraete et al., 2011). See also Figure S2.

for hCSF-1R$_{D3}$ (Figure S1A). Such structural plasticity in hCSF-1R$_{D3}$ may serve in terms of not only ensuring specificity and fidelity of binding to cognate cytokine ligands but also enabling correct positioning of the membrane-proximal regions of hCSF-1R to form an active signaling assembly.

Crystal Structure of the Human CSF-1:CSF-1R Extracellular Complex

To enable crystallographic studies of the complete hCSF-1:CSF-1R extracellular assembly, we produced glycosylated hCSF-1R$_{D1-D5}$ in transiently transfected HEK293T cells in the presence of the glycosylation inhibitor kifunensine (Chang et al., 2007) and reconstituted the hCSF-1:CSF-1R$_{D1-D5}$ complex as previously described (Elegheert et al., 2011; Felix et al., 2013). Attempts to further trim N-linked glycosylation in hCSF-1R$_{D1-D5}$ using EndoH led to recombinant receptor with dramatically lowered solubility and stability.

The crystal structure of the hCSF-1:CSF-1R$_{D1-D5}$ complex determined to 6.8 Å resolution features a 2-fold-symmetric assembly in which the ternary encounter complex (Figure 1A) is mounted on either side to a nearly linear stacking of the membrane-proximal domains D4 and D5, bringing the C-terminal ends of adjacent D5 to 40 Å from each other (Figure 2A; Table 1; Figure S2). Such geometry is possible due to the elbow-like arrangement of D3 and D4 domains, which come together at nearly 90° at the D3-D4 junction. Interestingly, analysis and modeling of our crystal structure against SAXS data showed that in the structure of the glycosylated complex in solution, hCSF-1R$_{D1}$ swings outward away from its collapsed interaction with hCSF-1R$_{D2}$ observed in the crystal structure (Figure 3A).

With the support of orthogonal structural information via single-particle EM analysis of the complex (Elegheert et al., 2011) (Figure 3B), we propose that hCSF-1R$_{D1}$ is inherently flexible about the D1-D2 linker, which may have functional implications. We note that analogous flexibility in D1 has also been observed in Flt3, another member of the RTKIII family (Verstraete et al., 2011).

Arguably, the hallmark of the complete ectodomain complex centers at the receptor-receptor interaction interface established between dimerized D4 domains (Figure 2A). While our crystallographic refinement of hCSF-1:CSF-1R$_{D1-D5}$ at 6.8 Å resolution was limited to rigid-body refinement protocols, the two dimerized D4 modules approached each other to optimal distances to enable salt bridges between R370 and E375 across the dimer interface via the main side-chain rotamers of each type of amino acid residue (Figure 2A, inset). Analogous homotypic receptor interactions have been proposed to be important for the activation of KIT (Reshetnyak et al., 2013, 2015; Yuzawa et al., 2007) (Figure 2B, inset), platelet-derived growth factor receptor β (PDGFRβ) (Yang et al., 2008), and vascular endothelial growth factor receptor (VEGFR) 1, 2, and 3 (Yang et al., 2010), and can be traced to a sequence fingerprint in the *EF* loop of D4 in RTKIII and D7 in the closely related RTKV, except from Flt3 (Figure 2C; Figure 2D). For instance, alanine point mutations of R381 and E386 in D4 of human KIT (Yuzawa et al., 2007), R385 and E390 in D4 of human PDGFRβ (Yang et al., 2008) and R726 and D731 in D7 of human VEGFR2 (Yang et al., 2010) compromise cytokine-driven receptor activation. Thus, the absence of homotypic interactions in Flt3 (Verstraete et al., 2011), which lacks this sequence cassette (Figure 2D), and structural
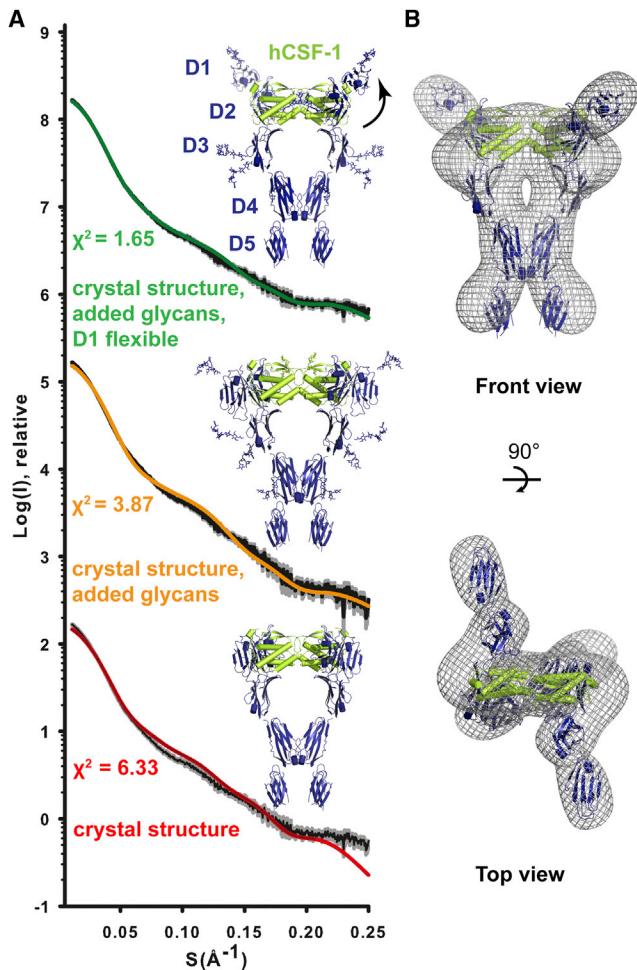
Figure 3. SAXS Analysis of the hCSF-1:CSF-1R$_{D1-D5}$ Complex

(A) Calculated SASREF/CRYSOL curves (colored) and their corresponding fits to the experimental data (black) are shown on a relative scale for the hCSF-1:CSF-1R$_{D1-D5}$ crystal structure (red curve), the hCSF-1:CSF-1R$_{D1-D5}$ crystal structure after adding N-glycans in SASREF (orange curve), followed by allowing D1 to move as a rigid body (green curve).

(B) Comparison of the hybrid X-ray/SAXS model for hCSF-1:CSF-1R$_{D1-D5}$ (green curve in A) and a 3D model obtained by EM for the hCSF-1:CSF-1R$_{D1-D5}$ complex (Elegheert et al., 2011) (EMD: 1977).

confirmation of homotypic receptor interactions mediated by such residues in human KIT, VEGFR2, and now in CSF-1R, greatly fortifies the expectation that cytokine-driven assemblies of PDGFRα and PDGFRβ will also display such structural features.

## Dimeric hCSF-1 Adopts an Active Conformation upon Binding to hCSF-1R

Considering the extensive interaction interface established between hCSF-1 and hCSF-1R, we were intrigued by the conspicuous absence of conformational changes at the side-chain level in hCSF-1 upon complex formation. In fact, comparison of receptor-bound hCSF-1 with five copies of unbound hCSF-1 (Elegheert et al., 2012) shows that only a handful of residues involved in receptor interactions undergo local side-chain rear-

rangements, while all other structural elements involved in receptor binding appear to be projected for binding as preformed binding surfaces. However, each copy of unbound CSF-1 displays a different tilt along its 2-fold axis of symmetry. Upon binding to hCSF-1R, dimeric hCSF-1 undergoes a rigid-body butterfly-like collapse to lock into a single conformer (Figures 4A and 4B). It would thus appear that dimeric hCSF-1 inherently exists as a conformational ensemble and that its engagement in a signaling complex with cognate receptor results in the selection of the active state of the cytokine. On the other hand, the conformation of hCSF-1 observed in the complex with hCSF-1R$_{D1-D3}$ superimposes with the most open form of unbound hCSF-1 (Figure 4A), implying that dimeric hCSF-1 retains its conformational plasticity even after it engages in the ternary encounter complex. Remarkably, the immunomodulatory viral protein BARF1 appears to play into the conformational states of dimeric hCSF-1 by binding precisely at the pivot point of the inter-subunit hinge on the opposite side of the cognate receptor interaction sites to lock the cytokine into a conformation that is unable to bind to cognate hCSF-1R (Figure 4C) (Elegheert et al., 2012). This observation had offered a first clue of an allosteric mechanism in the modulation of hCSF-1 activity and the possible role of inter-subunit plasticity of dimeric hCSF-1 in signaling. We note that hCSF-1 bound to BARF1 is identical to the collapsed conformation of unbound hCSF-1R and differs markedly from hCSF-1 bound to hCSF-1R$_{D1-D5}$ (Figure 4C). Thus, such structural benchmarking using cognate and noncognate complexes of hCSF-1 seals the notion that dimeric hCSF-1 can be directed to adopt active and inactive states.

DISCUSSION

The structures of human CSF-1:CSF-1R complexes presented here provide the necessary framework to consolidate prior biochemical, biophysical, and structural studies on CSF-1R complexes (Chen et al., 2008; Elegheert et al., 2011, 2012; Lin et al., 2008; Liu et al., 2012; Ma et al., 2012) to a synthesis of CSF-1R activation principles (Figure 5A). In addition, our work offers a mechanistic rationale for two recently uncovered modes of antagonism against hCSF-1 and hCSF-1R, respectively (Elegheert et al., 2012; Ries et al., 2014).

Previously, interaction studies employing an engineered monomeric variant of hCSF-1, dimeric hCSF-1, and truncation ectodomain variants of hCSF-1R (Elegheert et al., 2012) led to a quantitative deconvolution of the positive cooperativity in the hCSF-1:hCSF-1R complex into at least three levels of modular contributions: (1) an initial binary encounter complex between a subunit of hCSF-1 and a molecule of hCSF-1R ($K_D = 3$ μM); (2) a ternary encounter complex involving dimeric hCSF-1 and the cytokine-binding domains of hCSF1-R leading to a near 15-fold improvement in the K_D ($K_D = 213$ nM); and (3) the full ectodomain assembly stabilized by an additional 15-fold improvement in the K_D of the complex ($K_D = 14$ nM) mediated by receptor-receptor interactions via the membrane-proximal domains of hCSF-1R. Our structural studies have now shown that dimeric hCSF-1 utilizes largely preformed and extensive receptor binding sites targeting D2 and D3 in hCSF-1R to establish a ternary encounter complex that does not rely on receptor-receptor contacts (Figure 5A). In this context hCSF-1 maintains
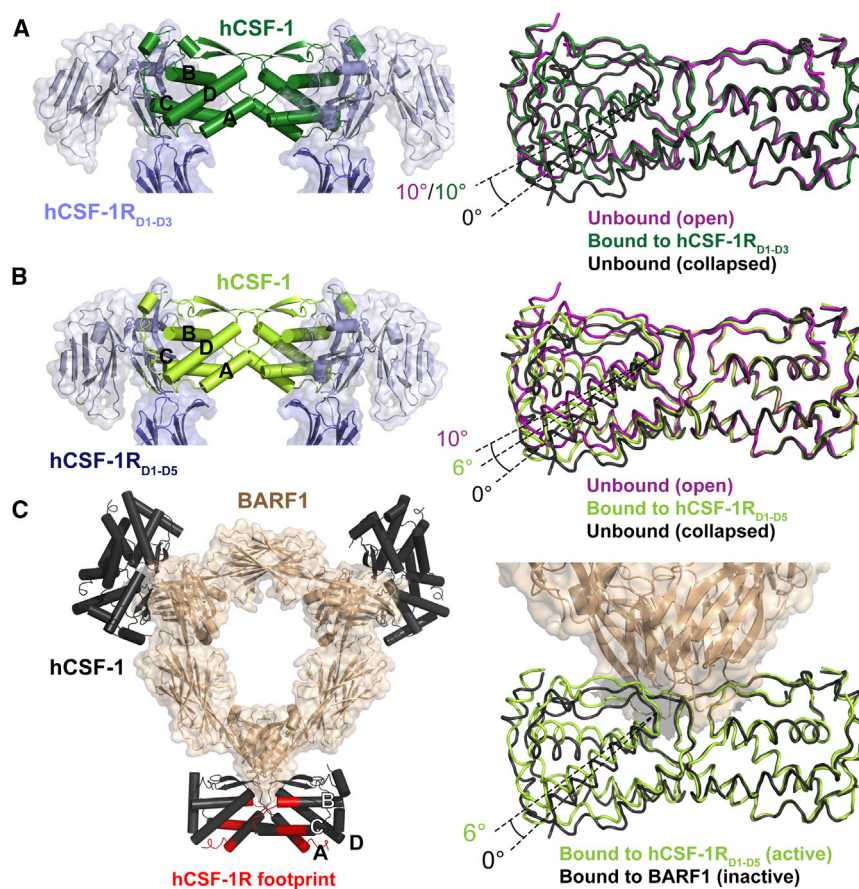
Figure 4. Conformational Plasticity of Dimeric hCSF-1

(A and B) Unbound structures of hCSF-1 (collapsed in black, open in purple; PDB: 3UF2) (Elegheert et al., 2012) are superimposed with hCSF-1 bound to hCSF-1R$_{D1-D3}$ (dark green) (A) and hCSF-1R$_{D1-D5}$ (lemon green) (B).

(C) hCSF-1 bound to viral BARF1 (PDB: 3UEZ) (Elegheert et al., 2012) compared with hCSF-1 bound to hCSF-1R$_{D1-D5}$. The hCSF-1R binding footprint on hCSF-1 is shown in red as a reference.

way dimeric activin activates transforming growth factor β family receptors (Greenwald et al., 2004), but has never been validated for cytokine:RTKIII complexes, although we did anticipate this possibility in a recent analysis (Verstraete and Savvides, 2012).

In a recent finding, the therapeutic monoclonal antibody RG7155 was shown to abrogate hCSF-1R signaling by binding with high affinity to the D4-D5 junction in the ectodomain of hCSF-1R (Ries et al., 2014). Our structural studies now provide the necessary insights to rationalize fully the antagonistic behavior of RG7155. Not only does RG7155 disrupt the D4-D4′ dimerization interface established in the hCSF-1:CSF-1R$_{D1-D5}$ complex, it does so by establishing salt bridges with E375 and R370 in hCSF-1R$_{D4}$ (Ries et al., 2014), which are essentially the centerfold of the D4-D4′ interface in the hCSF-1:CSF-1R complex (Figure 2). We note that similar antagonistic principles emerged from the development of therapeutic monoclonal antibodies against the D4-D5 segment of human KIT (Reshetnyak et al., 2013).

Our structure-based mechanistic proposal for the assembly of the hCSF-1:CSF-1R signaling assembly also provides opportunities to rationalize the ever-growing collection of somatic mutations that are identified in the extracellular segment of hCSF-1R (Forbes et al., 2015), which we can now readily map to the structure of the complex (Figure 5B). At the outset we propose that the role of such somatic mutations could be to stabilize either unbound or cytokine-bound forms of hCSF-1R or both, or to promote and/or predispose the adoption of active conformational states in hCSF-1R. Nonetheless, to date the only mutation shown to bestow transforming potential and ligand-independent activation upon hCSF-1R is L301S (Roussel et al., 1988), which localizes at end of the D3-D4 linker and contributes to the tip of the hydrophobic core in D4 facing D3 (Figure 5B). It is not yet clear how the L301S mutation could affect structure-function relationships in hCSF-1R, but one possibility is that it may enhance flexibility in the D3-D4 linker to promote receptor-receptor interactions. Of particular interest are several mutations that map to the membrane-proximal D4-D5 domain modules of hCSF-1R (Figure 5B). In fact, multiple somatic mutations in these regions have also been identified in all other RTKIIIs (reviewed in Verstraete and Savvides, 2012) and have been linked to

its inter-subunit plasticity (Figure 4A), which we propose is the key structural feature necessary to enable conformational sampling in hCSF-1R leading to the receptor dimerization interfaces between D4 domains. This leads to locking of hCSF-1 to its active state as manifested via the observed inter-subunit tilt in the extracellular complex (Figure 4B; Figure 5A). Thus, both the plasticity of hCSF-1 and the formation of homotypic receptor-receptor contacts are indispensable for the cooperative assembly of the hCSF-1R signaling complex (Figure 5A), although contributions from interactions between the membrane and intracellular domains of hCSF-1R would also be expected.

Remarkably, these are precisely the structural features targeted in two recently characterized non-cognate complexes of hCSF-1 and hCSF-1R$_{D1-D5}$, respectively, that result in antagonism of hCSF-1R signaling (Elegheert et al., 2012; Ries et al., 2014). In the first instance, the immunomodulatory protein BARF1 secreted by the Epstein-Barr virus binds with ultra-high affinity to the top of the dimer interface of hCSF-1 on the opposite side of the hCSF-1R binding epitope to lock dimeric hCSF-1 into a conformation that is incompetent to bind to hCSF-1R$_{D1-D5}$ (Figure 4C) (Elegheert et al., 2012). Such allosteric inactivation of dimeric hCSF-1 provides cross-validation of our proposal that conformational freedom of dimeric hCSF-1 is a requisite for its ability to drive the assembly of signaling complexes with hCSF-1R. Thus, a picture emerges whereby dimeric hCSF-1 can adopt active versus inactive states. Such a link between structural plasticity and signaling capacity is reminiscent of the
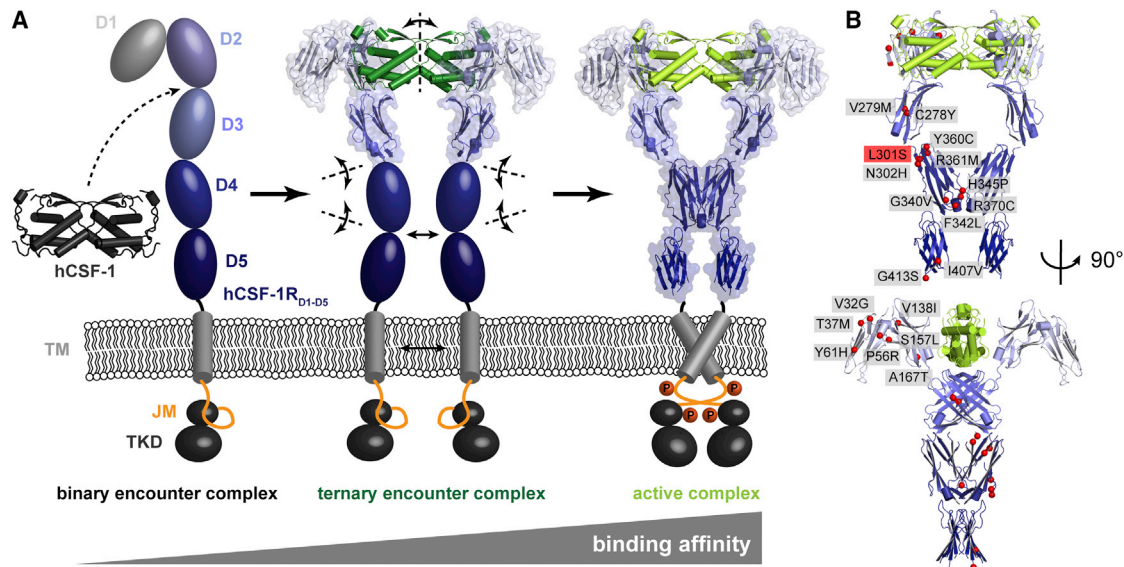
Figure 5. Mapping of Mechanistic Principles in Wild-Type and Oncogenic hCSF-1R

(A) Mechanism of hCSF-1R activation by hCSF-1. Binding affinities for the binary encounter, ternary encounter, and active complexes are shown on a relative scale.

(B) Mapping of confirmed somatic mutations (COSMIC, http://cancer.sanger.ac.uk) (Forbes et al., 2015) to the hCSF-1:CSF-1R$_{D1-D5}$ complex. The L301S mutation is highlighted in red to identify it as the only mutation to date with confirmed transforming properties.

mechanistic scenarios of enhanced receptor-receptor interactions in both constitutive and cytokine-driven receptor activation. Indeed, recent studies aiming to probe the effect of oncogenic mutations in D5 of human KIT have shown that they enhance the dimerization propensity of human KIT via D5-mediated homotypic receptor interfaces (Reshetnyak et al., 2015). Intriguingly, many mutations map to hCSF-1R$_{D1}$, which we have shown extends away from the complex in solution, and for which a functional annotation remains elusive.

Finally, we are left to wonder whether the mechanistic recapitulation of hCSF-1R activation driven by hCSF-1, in particular its reliance on hCSF-1 plasticity, also applies to hIL-34. Recent structural studies at low resolution have shown that the two cytokines establish strikingly similar extracellular assemblies with hCSF-1R activation (Felix et al., 2013), and we have shown here that both have evolved to respond to common binding principles that meet the geometric requirements of hCSF-1R. Given that the membrane-proximal domains in hCSF-1R also contribute at least one order of magnitude to the affinity of the extracellular complex driven by IL-34 (Chen et al., 2008; Liu et al., 2012; Ma et al., 2012) and the fact that hIL-34 also displays plasticity in its dimeric assembly as evidenced in its complex with Fab fragments (Ma et al., 2012), we are led to propose that the mechanistic principles we have derived for CSF-1 assemblies would be congruent with IL-34-driven complexes.

EXPERIMENTAL PROCEDURES

Recombinant Human CSF-1 and hCSF-1:CSF-1R Complexes

Recombinant hCSF-1 (Uniprot: P09603, α-splice variant, residues 1–149) was expressed via the pET-15b vector (Novagen) in the BL21(DE3) RosettaGami B (Novagen) *Escherichia coli* strain and refolded from inclusion bodies (Elegheert et al., 2011; Verstraete et al., 2009). Refolded hCSF-1 was purified by immobilized metal affinity chromatography (IMAC) using a prepacked 5-ml Ni-NTA Superflow cartridge (Qiagen). Immobilized hCSF-1 was washed with 50 mM NaH$_2$PO$_4$, 300 mM NaCl, and 15 mM imidazole (pH 7.0), and eluted with 50 mM NaH$_2$PO$_4$, 300 mM NaCl, 500 mM imidazole (pH 7.0). Protein fractions were pooled and further purified by SEC using a Prep-Grade Hiload 16/60 SD75 column (GE Healthcare) equilibrated with HEPES-buffered saline buffer (HBS; 20 mM HEPES [pH 7.5], 150 mM NaCl). Next, the N-terminal His$_6$ tag was removed by 1 unit of biotinylated thrombin (Novagen) per milligram of hCSF-1, followed by overnight incubation at room temperature. Biotinylated thrombin was removed with streptavidin-agarose beads (Novagen) at room temperature for 30 min followed by centrifugation at 500 × g. hCSF-1 was further purified to remove the cleaved N-terminal His$_6$ tag via a second SEC purification step. Purified hCSF-1 was concentrated to 1 mg/ml aliquots and flash-frozen for later use. Expression constructs corresponding to hCSF-1R$_{D1-D3}$ (residues 1–296) and hCSF-1R$_{D1-D5}$ (residues 1–503) (Uniprot: P07333), each with their native secretion signal, were cloned into the pHLsec vector for expression with a C-terminal His$_6$-tag (Aricescu et al., 2006). Based on the hCSF-1R$_{D1-D3}$ construct, four glycosylation mutants were designed as follows: N73Q, N153Q, N240Q, and N275Q. hCSF-1R$_{D1-D3}$ constructs were transiently transfected in HEK293T, HEK293S GnTI$^{-/-}$ (Reeves et al., 2002), and HEK293S GlycoDelete (Meuris et al., 2014), and 3.6 mM of valproic acid was added to the expression medium (Backliwal et al., 2008). Expression medium was harvested after 5 days and loaded onto a Talon FF column (Clontech). After IMAC purification using the same buffers as described for hCSF-1, purified hCSF-1R$_{D1-D3}$ glycosylation mutants were further purified by SEC on a Prep-Grade Hiload 16/60 SD200 column (GE Healthcare) equilibrated with HBS. To generate hCSF-1:CSF-1R$_{D1-D3}$ complexes, recombinant hCSF-1 (with cleaved N-terminal His$_6$ tag) was added in a 2:1 molar excess to hCSF-1R$_{D1-D3}$ glycosylation mutants, followed by a final SEC run. hCSF-1R$_{D1-D5}$ was expressed in HEK293T cells in the presence of kifunensine (Chang et al., 2007) and purified by IMAC using Talon beads (Clontech). After addition of a molar excess of hCSF-1, hCSF-1:CSF-1R$_{D1-D5}$ was further purified by SEC on a Superdex 200 16/60 column (GE Healthcare) equilibrated with HBS. For deglycosylation, hCSF-1:CSF-1R$_{D1-D5}$ was treated overnight with endoglycosidase

F1 (1:100 w/w at 294 K). Deglycosylated hCSF-1:CSF-1R$_{D1-D5}$ was purified further via SEC in HBS buffer.

Crystallization and X-Ray Data Collection
hCSF-1:CSF-1R$_{D1-D3}$

Purified complexes of refolded hCSF-1 and each of the hCSF-1R$_{D1-D3}$ glycosylation mutants expressed in HEK293T, HEK293S GnTI$^{-/-}$, and HEK293S GlycoDelete cells were concentrated to approximately 7 mg/ml and subjected to initial crystallization trials, both in a sitting- and hanging-drop vapor-diffusion geometry using a Mosquito robot (TTP LabTech). The best diffracting crystals were obtained from hCSF-1R$_{D1-D3}$ N240Q expressed in HEK293S GlycoDelete cells. Brick-shaped crystals grew at 20°C after mixing 100 nl of hCSF-1:CSF-1R$_{D1-D3}$ N240Q (7.4 mg/ml) with 100 nl of reservoir solution containing 0.2 M lithium sulfate monohydrate, 0.1 M Tris (pH 8.5), and 28% w/v PEG3350. Prior to X-ray data collection, crystals were stepwise incubated in stabilizing solution containing 35% v/w PEG3350 and 5% ethylene glycol. Cryoprotected crystals were subsequently flash-frozen in liquid nitrogen and diffraction data were collected to 2.8 Å at the ID23-1 beamline of the ESRF (Grenoble, France).

hCSF-1:CSF-1R$_{D1-D5}$

Hexagonal rod-like crystals of hCSF-1:CSF-1R$_{D1-D5}$ were grown via sitting-drop vapor-diffusion geometry at 20°C by mixing 1 μl of the complex at 5 mg/ml and 1 μl of a reservoir solution containing 0.1 M NaCl, 0.1 M Tris (pH 7.0), and 6% PEG20000. Crystals were cryoprotected using stabilizing solution containing 30% v/v of sugar mixture (10% v/v D-glucose, 10% v/v sucrose, 10% v/v sorbitol), and flash-frozen in liquid nitrogen. Diffraction data to 6.8 Å were collected at the PXI beamline at the SLS (Villigen, Switzerland). All data were processed with XDS (Kabsch, 2010).

Crystal Structure Determination and Refinement
hCSF-1:CSF-1R$_{D1-D3}$

The data were processed in space group $I4_1$ ($a = 142.99$ Å, $b = 142.99$ Å, $c = 139.32$ Å), and the structure was solved by maximum-likelihood molecular replacement (MR) in Phaser (McCoy et al., 2007) using the crystal structure of hCSF-1 (PDB: 3UF2) (Elegheert et al., 2012) and hCSF-1R$_{D1-D3}$ as found in the hIL-34:CSF-1R$_{D1-D3}$ crystal structure (PDB: 4DKD) (Ma et al., 2012). A single MR solution was found for a ternary complex containing one CSF-1 dimer bound by two CSF-1R$_{D1-D3}$ receptor molecules in the asymmetric unit. Initial refinement was performed in BUSTER (Blanc et al., 2004) using rigid-body refinement in the first of five macrocycles. The resulting electron density maps showed clear density for hCSF-1 and two copies of hCSF-1R$_{D1-D2}$, whereas the density for two hCSF-1R$_{D3}$ domains was only readily interpretable at the hCSF-1:CSF-1R$_{D3}$ interface. The electron density was greatly improved by allowing hCSF-1R$_{D3}$ to refine as a separate entity, consistent with the plasticity of hCSF-1R$_{D3}$. Additional refinement steps were carried out in PHENIX (Adams et al., 2010) using individual B-factor refinement with TLS (translation/libration/screw), XYZ refinement, occupancy refinement, optimized X-ray/geometry weight, non-crystallographic symmetry restraints, mask parameter refinement, and removal of some flexible solvent-exposed side chains for which no clear density was visible. Lastly, glycan chains on Asn73, Asn45, Asn153, and Asn275 were added to the model, which was further refined to completion in PHENIX (R/R_{free}: 22.31%/26.13%) and validated using MolProbity software (Chen et al., 2010).

hCSF-1:CSF-1R$_{D1-D5}$

The data were processed in space group $P6_122$ ($a = 281.47$ Å, $b = 281.47$ Å, $c = 91.17$ Å, $\alpha = \beta = 90°$, $\gamma = 120°$) and ellipsoidally truncated and anisotropically scaled (Strong et al., 2006). Recommended resolution limits along the reciprocal unit cell axes a^*, b^*, and c^* were 7.4, 7.6, and 6.8 Å, respectively. Using our structure of hCSF-1:CSF-1R$_{D1-D3}$ to 2.8 Å resolution as a search model, a single solution was found using maximum-likelihood MR in Phaser for one subunit of hCSF-1 and one molecule of hCSF-1R$_{D1-D3}$ in the asymmetric unit. The ensuing ternary complex is generated by a crystallographic 2-fold axis of symmetry along the unit cell b axis. Based on the composition of the asymmetric unit, the solvent content of the crystal was estimated (Kantardjieff and Rupp, 2003) to be unusually high (~85%), which may rationalize the poor diffraction quality of the crystals. Using the atomic coordinates for hCSF-1R$_{D4}$ (PDB: 4LIQ) (Ries et al., 2014), maximum-likelihood MR in Phaser gave a single solution for the placement of D4, where two adjacent D4s (symmetry mates) are

contacting each other. Due to obvious main-chain clashes, the rotamer of Arg370 (taken from the Fab:hCSF-1R$_{D4}$ complex, PDB: 4LIQ) was modeled to its most predominant rotamer in Coot. This led readily to a salt bridge between Arg370 and Glu375 of an opposing hCSF-1R$_{D4}$ analogous to the one observed between D4 domains in the SCF:KIT complex (Yuzawa et al., 2007). For hCSF-1R$_{D5}$, MR in Phaser did not yield a solution, although density for D5 was clearly visible after one round of rigid-body refinement in PHENIX. Manual placement of hCSF-1R$_{D5}$ followed by refinement in PHENIX using rigid-body refinement, occupancy refinement, group B-factor refinement with TLS, optimized X-ray/geometry weight, and mask parameter refinement finally resulted in R/R_{free} values of 32.63%/35.93%. Recalculation of the R/R_{free} values using the full data range resulted in R/R_{free} values of 34.29%/36.19%.

Small-Angle X-Ray Scattering

SAXS data acquisition for the hCSF-1:CSF-1R$_{D1-D5}$ complex and subsequent data processing were performed as described by Elegheert et al. (2011) and Felix et al. (2013), respectively. CRYSOL (Petoukhov et al., 2012; Svergun et al., 1995) was used to calculate a theoretical scattering curve from the hCSF-1:CSF-1R$_{D1-D5}$ crystal structure as well as its discrepancy from the experimental SAXS data. Rigid-body refinement of the hCSF-1:CSF-1R$_{D1-D5}$ complex was performed using the online version of SASREF (Petoukhov et al., 2012; Petoukhov and Svergun, 2005). For each run, data to 0.25 Å^{-1} was used while imposing P2 symmetry. The structure of hCSF-1:CSF-1R$_{D1-D5}$ lacking D1 was taken as a starting rigid-body core. D1 was added as a separate rigid body with a contact restraint of 4 Å between its C and the N terminus of hCSF-1R$_{D2-D5}$, as well as five N-linked glycans containing a "dummy" asparagine residue (Asn-GlcNAc$_2$Man$_5$) with 1-Å restraints to the Cα of truncated asparagine residues on hCSF-1R$_{D2-D5}$ (N73, N153, N240, N275, and N353). The fit of the model to the experimental data via SASREF yielded χ^2 values of 1.65, 3.0, and 1.5 in SASREF, CRYSOL, and FoxS (Schneidman-Duhovny et al., 2013), respectively.

ACCESSION NUMBERS

Crystallographic coordinates and structure factors have been deposited in the wwPDB with accession codes PDB: 4WRL (hCSF-1:hCSF-1R$_{D1-D3}$) and 4WRM (hCSF-1:hCSF-1R$_{D1-D5}$). The SAXS model for hCSF-1:hCSF-1R$_{D1-D5}$ and corresponding scattering curve and fit have been deposited in the Small-Angle Scattering Biological Data Bank with accession code SASBDB: SASDAR6.

SUPPLEMENTAL INFORMATION

Supplemental Information includes two figures and one table and can be found with this article online at http://dx.doi.org/10.1016/j.str.2015.06.019.

AUTHOR CONTRIBUTIONS

ACKNOWLEDGMENTS

REFERENCES

Adams, P.D., Afonine, P.V., Bunkoczi, G., Chen, V.B., Davis, I.W., Echols, N., Headd, J.J., Hung, L.W., Kapral, G.J., Grosse-Kunstleve, R.W., et al. (2010). PHENIX: a comprehensive Python-based system for macromolecular structure solution. Acta Crystallogr. D Biol. Crystallogr. 66, 213–221.

Aricescu, A.R., Lu, W., and Jones, E.Y. (2006). A time- and cost-efficient system for high-level protein production in mammalian cells. Acta Crystallogr. D Biol. Crystallogr. 62, 1243–1250.

Backliwal, G., Hildinger, M., Kuettel, I., Delegrange, F., Hacker, D.L., and Wurm, F.M. (2008). Valproic acid: a viable alternative to sodium butyrate for enhancing protein expression in mammalian cell cultures. Biotechnol. Bioeng. 101, 182–189.

Blanc, E., Roversi, P., Vonrhein, C., Flensburg, C., Lea, S.M., and Bricogne, G. (2004). Refinement of severely incomplete structures with maximum likelihood in BUSTER-TNT. Acta Crystallogr. D Biol. Crystallogr. 60, 2210–2221.

Chang, V.T., Crispin, M., Aricescu, A.R., Harvey, D.J., Nettleship, J.E., Fennelly, J.A., Yu, C., Boles, K.S., Evans, E.J., Stuart, D.I., et al. (2007). Glycoprotein structural genomics: solving the glycosylation problem. Structure 15, 267–273.

Chen, X., Liu, H., Focia, P.J., Shim, A.H., and He, X. (2008). Structure of macrophage colony stimulating factor bound to FMS: diverse signaling assemblies of class III receptor tyrosine kinases. Proc. Natl. Acad. Sci. USA 105, 18267–18272.

Chen, V.B., Arendall, W.B., 3rd, Headd, J.J., Keedy, D.A., Immormino, R.M., Kapral, G.J., Murray, L.W., Richardson, J.S., and Richardson, D.C. (2010). MolProbity: all-atom structure validation for macromolecular crystallography. Acta Crystallogr. D Biol. Crystallogr. 66, 12–21.

Chihara, T., Suzu, S., Hassan, R., Chutiwitoonchai, N., Hiyoshi, M., Motoyoshi, K., Kimura, F., and Okada, S. (2010). IL-34 and M-CSF share the receptor Fms but are not identical in biological activity and signal activation. Cell Death Differ. 17, 1917–1927.

Chitu, V., and Stanley, E.R. (2006). Colony-stimulating factor-1 in immunity and inflammation. Curr. Opin. Immunol. 18, 39–48.

Elegheert, J., Desfosses, A., Shkumatov, A.V., Wu, X., Bracke, N., Verstraete, K., Van Craenenbroeck, K., Brooks, B.R., Svergun, D.I., Vergauwen, B., et al. (2011). Extracellular complexes of the hematopoietic human and mouse CSF-1 receptor are driven by common assembly principles. Structure 19, 1762–1772.

Elegheert, J., Bracke, N., Pouliot, P., Gutsche, I., Shkumatov, A.V., Tarbouriech, N., Verstraete, K., Bekaert, A., Burmeister, W.P., Svergun, D.I., et al. (2012). Allosteric competitive inactivation of hematopoietic CSF-1 signaling by the viral decoy receptor BARF1. Nat. Struct. Mol. Biol. 19, 938–947.

Felix, J., Elegheert, J., Gutsche, I., Shkumatov, A.V., Wen, Y., Bracke, N., Pannecoucke, E., Vandenberghe, I., Devreese, B., Svergun, D.I., et al. (2013). Human IL-34 and CSF-1 establish structurally similar extracellular assemblies with their common hematopoietic receptor. Structure 21, 528–539.

Forbes, S.A., Beare, D., Gunasekaran, P., Leung, K., Bindal, N., Boutselakis, H., Ding, M., Bamford, S., Cole, C., Ward, S., et al. (2015). COSMIC: exploring the world's knowledge of somatic mutations in human cancer. Nucleic Acids Res. 43, D805–D811.

Greenwald, J., Vega, M.E., Allendorph, G.P., Fischer, W.H., Vale, W., and Choe, S. (2004). A flexible activin explains the membrane-dependent cooperative assembly of TGF-beta family receptors. Mol. Cell 15, 485–489.

Hume, D.A., and MacDonald, K.P.A. (2012). Therapeutic applications of macrophage colony-stimulating factor-1 (CSF-1) and antagonists of CSF-1 receptor (CSF-1R) signaling. Blood 119, 1810–1820.

Kabsch, W. (2010). XDS. Acta Crystallogr. D Biol. Crystallogr. 66, 125–132.

Kantardjieff, K.A., and Rupp, B. (2003). Matthews coefficient probabilities: improved estimates for unit cell contents of proteins, DNA, and protein-nucleic acid complex crystals. Protein Sci. 12, 1865–1871.

Lemmon, M.A., and Schlessinger, J. (2010). Cell signaling by receptor tyrosine kinases. Cell 141, 1117–1134.

Lin, H., Lee, E., Hestir, K., Leo, C., Huang, M., Bosch, E., Halenbeck, R., Wu, G., Zhou, A., Behrens, D., et al. (2008). Discovery of a cytokine and its receptor by functional screening of the extracellular proteome. Science 320, 807–811.

Liu, H., Leo, C., Chen, X., Wong, B.R., Williams, L.T., Lin, H., and He, X. (2012). The mechanism of shared but distinct CSF-1R signaling by the non-homologous cytokines IL-34 and CSF-1. Biochim. Biophys. Acta 1824, 938–945.

Ma, X., Lin, W.Y., Chen, Y., Stawicki, S., Mukhyala, K., Wu, Y., Martin, F., Bazan, J.F., and Starovasnik, M.A. (2012). Structural basis for the dual recognition of helical cytokines IL-34 and CSF-1 by CSF-1R. Structure 20, 676–687.

Masteller, E.L., and Wong, B.R. (2014). Targeting IL-34 in chronic inflammation. Drug Discov. Today 19, 1212–1216.

McCoy, A.J., Grosse-Kunstleve, R.W., Adams, P.D., Winn, M.D., Storoni, L.C., and Read, R.J. (2007). Phaser crystallographic software. J. Appl. Crystallogr. 40, 658–674.

Meuris, L., Santens, F., Elson, G., Festjens, N., Boone, M., Dos Santos, A., Devos, S., Rousseau, F., Plets, E., Houthuys, E., et al. (2014). GlycoDelete engineering of mammalian cells simplifies N-glycosylation of recombinant proteins. Nat. Biotechnol. 32, 485–489.

Muller, P.A., Koscso, B., Rajani, G.M., Stevanovic, K., Berres, M.L., Hashimoto, D., Mortha, A., Leboeuf, M., Li, X.M., Mucida, D., et al. (2014). Crosstalk between muscularis macrophages and enteric neurons regulates gastrointestinal motility. Cell 158, 300–313.

Nandi, S., Gokhan, S., Dai, X.M., Wei, S., Enikolopov, G., Lin, H., Mehler, M.F., and Stanley, E.R. (2012). The CSF-1 receptor ligands IL-34 and CSF-1 exhibit distinct developmental brain expression patterns and regulate neural progenitor cell maintenance and maturation. Dev. Biol. 367, 100–113.

Pandit, J., Bohm, A., Jancarik, J., Halenbeck, R., Koths, K., and Kim, S.H. (1992). Three-dimensional structure of dimeric human recombinant macrophage colony-stimulating factor. Science 258, 1358–1362.

Petoukhov, M.V., and Svergun, D.I. (2005). Global rigid body modeling of macromolecular complexes against small-angle scattering data. Biophysical J. 89, 1237–1250.

Petoukhov, M.V., Franke, D., Shkumatov, A.V., Tria, G., Kikhney, A.G., Gajda, M., Gorba, C., Mertens, H.D.T., Konarev, P.V., and Svergun, D.I. (2012). New developments in the ATSAS program package for small-angle scattering data analysis. J. Appl. Crystallogr. 45, 342–350.

Pollard, J.W. (2009). Trophic macrophages in development and disease. Nat. Rev. Immunol. 9, 259–270.

Reeves, P.J., Callewaert, N., Contreras, R., and Khorana, H.G. (2002). Structure and function in rhodopsin: high-level expression of rhodopsin with restricted and homogeneous N-glycosylation by a tetracycline-inducible N-acetylglucosaminyltransferase I-negative HEK293S stable mammalian cell line. Proc. Natl. Acad. Sci. USA 99, 13419–13424.

Reshetnyak, A.V., Nelson, B., Shi, X., Boggon, T.J., Pavlenco, A., Mandel-Bausch, E.M., Tome, F., Suzuki, Y., Sidhu, S.S., Lax, I., et al. (2013). Structural basis for KIT receptor tyrosine kinase inhibition by antibodies targeting the D4 membrane-proximal region. Proc. Natl. Acad. Sci. USA 110, 17832–17837.

Reshetnyak, A.V., Opatowsky, Y., Boggon, T.J., Folta-Stogniew, E., Tome, F., Lax, I., and Schlessinger, J. (2015). The strength and cooperativity of KIT ectodomain contacts determine normal ligand-dependent stimulation or oncogenic activation in cancer. Mol. Cell 57, 191–201.

Ries, C.H., Cannarile, M.A., Hoves, S., Benz, J., Wartha, K., Runza, V., Rey-Giraud, F., Pradel, L.P., Feuerhake, F., Klaman, I., et al. (2014). Targeting

tumor-associated macrophages with anti-CSF-1R antibody reveals a strategy for cancer therapy. Cancer Cell *25*, 846–859.

Roussel, M.F., Downing, J.R., Rettenmier, C.W., and Sherr, C.J. (1988). A point mutation in the extracellular domain of the human CSF-1 receptor (c-fms proto-oncogene product) activates its transforming potential. Cell *55*, 979–988.

Schneidman-Duhovny, D., Hammel, M., Tainer, J.A., and Sali, A. (2013). Accurate SAXS profile computation and its assessment by contrast variation experiments. Biophysical J. *105*, 962–974.

Sherr, C.J., Rettenmier, C.W., Sacca, R., Roussel, M.F., Look, A.T., and Stanley, E.R. (1985). The c-fms proto-oncogene product is related to the receptor for the mononuclear phagocyte growth factor, CSF-1. Cell *41*, 665–676.

Stanley, E.R., and Chitu, V. (2014). CSF-1 receptor signaling in myeloid cells. Cold Spring Harb. Perspect. Biol. *6*, a021857.

Strong, M., Sawaya, M.R., Wang, S., Phillips, M., Cascio, D., and Eisenberg, D. (2006). Toward the structural genomics of complexes: crystal structure of a PE/PPE protein complex from *Mycobacterium tuberculosis*. Proc. Natl. Acad. Sci. USA *103*, 8060–8065.

Svergun, D., Barberato, C., and Koch, M.H.J. (1995). CRYSOL-a program to evaluate X-ray solution scattering of biological macromolecules from atomic coordinates. J. Appl. Crystallogr. *28*, 768–773.

Taylor, E.W., Fear, A.L., Bohm, A., Kim, S.H., and Koths, K. (1994). Structure-function studies on recombinant human macrophage colony-stimulating factor (M-CSF). J. Biol. Chem. *269*, 31171–31177.

Verstraete, K., and Savvides, S.N. (2012). Extracellular assembly and activation principles of oncogenic class III receptor tyrosine kinases. Nat. Rev. Cancer *12*, 753–766.

Verstraete, K., Koch, S., Ertugrul, S., Vandenberghe, I., Aerts, M., Vandriessche, G., Thiede, C., and Savvides, S.N. (2009). Efficient production of bioactive recombinant human Flt3 ligand in *E. coli*. Protein J. *28*, 57–65.

Verstraete, K., Vandriessche, G., Januar, M., Elegheert, J., Alexander, V., Desfosses, A., Craenenbroeck, K.V., Svergun, D.I., Gutsche, I., Vergauwen, B., et al. (2011). Structural insights into the extracellular assembly of the hematopoietic Flt3 signaling complex. Blood *118*, 60–68.

Wei, S., Nandi, S., Chitu, V., Yeung, Y.-G., Yu, W., Huang, M., Williams, L.T., Lin, H., and Stanley, E.R. (2010). Functional overlap but differential expression of CSF-1 and IL-34 in their CSF-1 receptor-mediated regulation of myeloid cells. J. Leukoc. Biol. *88*, 495–505.

Yang, Y., Yuzawa, S., and Schlessinger, J. (2008). Contacts between membrane proximal regions of the PDGF receptor ectodomain are required for receptor activation but not for receptor dimerization. Proc. Natl. Acad. Sci. USA *105*, 7681–7686.

Yang, Y., Xie, P., Opatowsky, Y., and Schlessinger, J. (2010). Direct contacts between extracellular membrane-proximal domains are required for VEGF receptor activation and cell signaling. Proc. Natl. Acad. Sci. USA *107*, 1906–1911.

Yuzawa, S., Opatowsky, Y., Zhang, Z., Mandiyan, V., Lax, I., and Schlessinger, J. (2007). Structural basis for activation of the receptor tyrosine kinase KIT by stem cell factor. Cell *130*, 323–334.